Frontiers of Optoelectronics (2022) 15:3
https://doi.org/10.1007/s12200-022-00003-w

Frontiers of Optoelectronics

RESEARCH ARTICLE

All-solid anti-resonant single crystal fibers

Jinmin Ding[1] · Fanchao Meng[1] · Xiaoting Zhao[1] · Xin Wang[2] · Shuqin Lou[2] · Xinzhi Sheng[1] · Luyun Yang[3] · Guangming Tao[3,4] · Sheng Liang[1]

Received: 12 May 2021 / Accepted: 18 June 2021

Abstract
In this paper, a novel all-solid anti-resonant single crystal fiber (AR-SCF) with high refractive index tubes cladding is proposed. By producing the cladding tubes with high refractive index material, the AR guiding mechanism can be realized for the SCF, which can reduce the mode number to achieve single-mode or few-mode transmission. The influences of different materials and structures on the confinement loss and effective guided mode number for wavelengths of 2–3 μm are investigated. Then, the optimal AR-SCF structures for different wavelengths are determined. Furthermore, the influences of different fabrication errors are analyzed. This work would provide insight to new opportunities in the novel design of SCFs by AR, which would greatly impact the fields of laser application, supercontinum generation, and SCF sensors.

Keywords Single crystal fiber (SCF) · Anti-resonant (AR) optical fiber · Few-mode fiber · Modal reduction · Confinement loss · Finite element method

1 Introduction

As a combination of bulk crystals and traditional fibers, single crystal fibers (SCFs) inherited the advantages of crystals, including high melting points, high thermal conductivity, high laser damage threshold, and good mechanical properties. They also carried the advantages of conventional optical fibers, such as having a large aspect ratio and specific surface area, both of which remarkably improve their thermal management capabilities [1, 2]. SCFs have been widely used in many fields due to their excellent comprehensive properties. As an outstanding fiber laser gain medium, SCFs are expected to have higher melting points, thermal conductivity, strength, laser damage threshold (500 times higher than that of silica), doping concentration, and a lower Brillouin gain coefficient [3–5]. Compared to silica fiber, sapphire SCF is a better platform for supercontinum generation due to its high transparency up to 5 μm, low material dispersion

✉ Guangming Tao
TAO@hust.edu.cn

✉ Sheng Liang
shliang@bjtu.edu.cn

Jinmin Ding
djinmin1996@163.com

Fanchao Meng
mfanchao@126.com

Xiaoting Zhao
xiaoting_zhao@163.com

Xin Wang
xin.wang@bjtu.edu.cn

Shuqin Lou
shqlou@bjtu.edu.cn

Xinzhi Sheng
xzhsheng@bjtu.edu.cn

Luyun Yang
luyunyang@gmail.com

1 Key Laboratory of Education Ministry on Luminescence and Optical Information Technology, National Physical Experiment Teaching Demonstration Center, Department of Physics, School of Science, Beijing Jiaotong University, Beijing 100044, China

2 School of Electronic and Information Engineering, Beijing Jiaotong University, Beijing 100044, China

3 Wuhan National Laboratory for Optoelectronics, Huazhong University of Science and Technology, Wuhan 430074, China

4 State Key Laboratory of Crystal Materials, Shandong University, Jinan 250100, China

Published online: 29 March 2022

in the 0.8–5 μm spectral range, and higher laser damage threshold [6, 7]. Furthermore, SCF-based sensors are the unique and effective solution in high-temperature, high-pressure, and chemically aggressive environments that require high temperature stability and transient response characteristics because of their high melting point, superb mechanical properties, and stable physical and chemical properties [8–11].

However, the SCFs are multi-mode without cladding, which leads to significant difficulties during application. Therefore, SCF cladding has been utilized to reduce the confinement loss (*CL*) and the number of effective guided modes to achieve the single-mode or few-mode transmission.

Current SCF cladding techniques are based on the principle of total reflection, also known as refractive index guiding, which is achieved by adjusting the refractive index of the cladding to be lower than that of the core. Therefore, it is common for cladding materials to have lower refractive indices and similar thermal expansion coefficients to that of the core. Effective cladding methods include the magnetron sputtering [12], Sol–Gel method [13, 14], liquid phase epitaxy [15], co-drawing laser heating pedestal growth (LHPG) [16–24], ion implantation [25–28], and micro-structure cladding [7, 29, 30].

The disadvantages of the existing refractive index guiding cladding techniques include the small bandwidth and requirement of high structure accuracy during preparation. However, other light-guiding mechanisms may aid in the potential advancement of SCF cladding. The anti-resonant (AR), or negative curvature, optical fibers with a cladding that consists of a single ring of tubes have sparked a lot of interest due to their low losses over a wide wavelength span, simple cladding structure, and freedom in design [31, 32].

In this paper, by designing an analogy of current air-glass AR hollow-core fiber structure, we have proposed and investigated an all-solid AR-SCF. The AR guiding can shed light on new opportunities for cladded all-solid SCFs with simple cladding structure, a potential SCF design with low *CL* and single or few mode transmission.

2 Design of anti-resonant single crystal fiber (AR-SCF)

2.1 Structures

Our proposed all-solid AR-SCF with single-ring tubes is shown in Fig. 1. As an analogy of the air-glass AR optical fiber structure, a single ring of the high refractive index material tubes (blue in Fig. 1) with diameter *d* and thickness *t* is embedded in the single crystal material (yellow in Fig. 1). The area in the center of the tubes is the core with the diameter *D*.

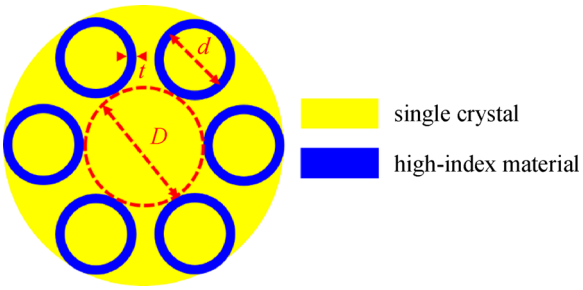

Fig. 1 Structure of all-solid AR-SCF with single-ring cladding tubes. *D*: diameter of core, *d*: diameter of the cladding-tube, and *t*: thickness of the cladding-tube

2.2 Materials

The optical and thermal parameters of the single crystal core and cladding materials are shown in Table 1.

3 Results and discussion

3.1 Numerical method

The AR-SCF was numerically investigated using the finite element method (FEM) with the circular perfectly matched layer (PML), which allowed us to calculate the value of *CL* according to the equations [33]:

$$CL = 8.686 \times k \times \mathrm{Im}\left(n_{\mathrm{eff}}\right), \tag{1}$$

$$k = \frac{2\pi}{\lambda}, \tag{2}$$

where $\mathrm{Im}(n_{\mathrm{eff}})$ is the imaginary parts of n_{eff}, λ is the wavelength.

For the step index fiber, the number of guided modes can be calculated using the following equations:

$$V = \pi \frac{d}{\lambda} NA, \tag{3}$$

$$NA = \sqrt{{n_1}^2 - {n_2}^2}, \tag{4}$$

$$M = \frac{4}{\pi^2} V^2, \tag{5}$$

where *d* is the fiber diameter, n_1 and n_2 are the refractive indices of the core and cladding tube, *NA* is the numerical aperture, and *M* is the number of modes. However, this

Table 1 Materials of the single crystal core and cladding tubes

Materials		Refractive index@2.8 μm	Melting point/°C
Single crystal	Sapphire (Al_2O_3)	1.7490–1.7170	2054
	Lutetium oxide	1.901	2510
	Y_2O_3	1.90–1.87	2439
	$MgAl_2O_4$	1.703–1.668	2250
	SiC	2.58–2.52	2830
	Nd:YAG	1.81	1970
	$LiNbO_3$	2.236–2.1615	1253
	BaB_2O_4	1.6556–1.6129	1060
Cladding-tubes	Lanthanide glass (S-LAN79)	2.0008	699
	AsS	2.35	180
	GeAsS	2.22	420
	GeS	2.11	380
	ZnS	2.19	1830
	As_2S_3	2.4218	197

method is ineffective for the AR-SCF due to significant errors calculated by Eq. (5). Therefore, we determined the number of guided modes by calculating the effective refractive and the *CL* difference between the higher order mode and the fundamental mode. If the *CL* of the higher order mode is three orders of magnitude greater than the *CL* of the fundamental mode, then the higher order mode is considered a less effective transmission mode.

3.2 Numerical results

The light-guiding in AR fibers is achieved by inhibited coupling between the core and cladding modes. The low loss transmission windows are determined by the cladding capillary thickness, according to the anti-resonant reflecting optical waveguide (ARROW) model. Then, one of the most important performances of AR-SCF is the *CL*, which relates to the leaky nature of the guided modes, is the dominant loss mechanism in the near infrared region.

First, in order to verify the anti-resonant light-guiding of AR-SCF, the *CL* with the thickness of cladding-tubes (t) from 0.2 to 4.0 μm at wavelength of 2.8 μm is shown in Fig. 2, with the structure parameters $n_1 = 1.89$, $n_2 = 2.20$, $D = 30$ μm, $d = 20$ μm.

As exhibited in Fig. 2, with the increase of t, the low *CL* changes periodically, namely characteristic of anti-resonant light-guiding. It is the anti-resonant state when t is 0.9, 2.1, and 3.5 μm, with *CL* less than 1×10^{-4} dB/m. When t is 0.3, 1.4, 2.6, and 3.9 μm, and *CL* is higher than 1 dB/m, the corresponding thickness of the cladding-tubes are ineffective in the achievement of light-guiding. There are four guide modes at the anti-resonant point and the normalized intensity profiles of the AR-SCF when t is 0.9 μm and the wavelength is 2.8 μm are shown in Fig. 3. The above results suggest that the all-solid AR-SCF can be achieved.

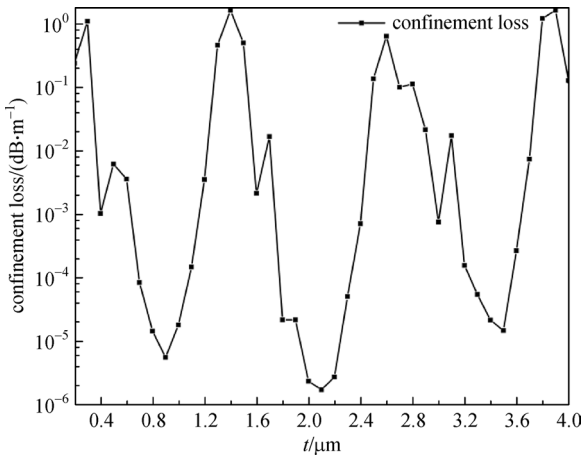

Fig. 2 Confinement loss (*CL*) with the thickness (t) of cladding-tube at wavelength of 2.8 μm. $n_1 = 1.89$, $n_2 = 2.20$, $D = 30$ μm, $d = 20$ μm

Figure 4 shows the relationship between *CL* and wavelength (range is 2–3 μm) for different t. When t is 0.9 μm, the value of *CL* initially decreases as the wavelength increases, then gradually increases after 2.7 μm. When t is 2.1 μm, the *CL* initially increases, then decreases, and finally increases again when the wavelength increases from 2.0 to 3.0 μm. The trend of *CL* adds an additional decrease when the wavelength increases from 2.0 to 2.1 μm, compared to when t is 2.1 and 3.5 μm. No obvious changes in *CL* are observed when the wavelength is 2.8 μm with different t, though the lowest *CL* can be obtained when $t = 0.9$ μm.

The relationship between *CL* and d in the cases of different t is reported in Fig. 5. The *CL* in Fig. 5 decreases as

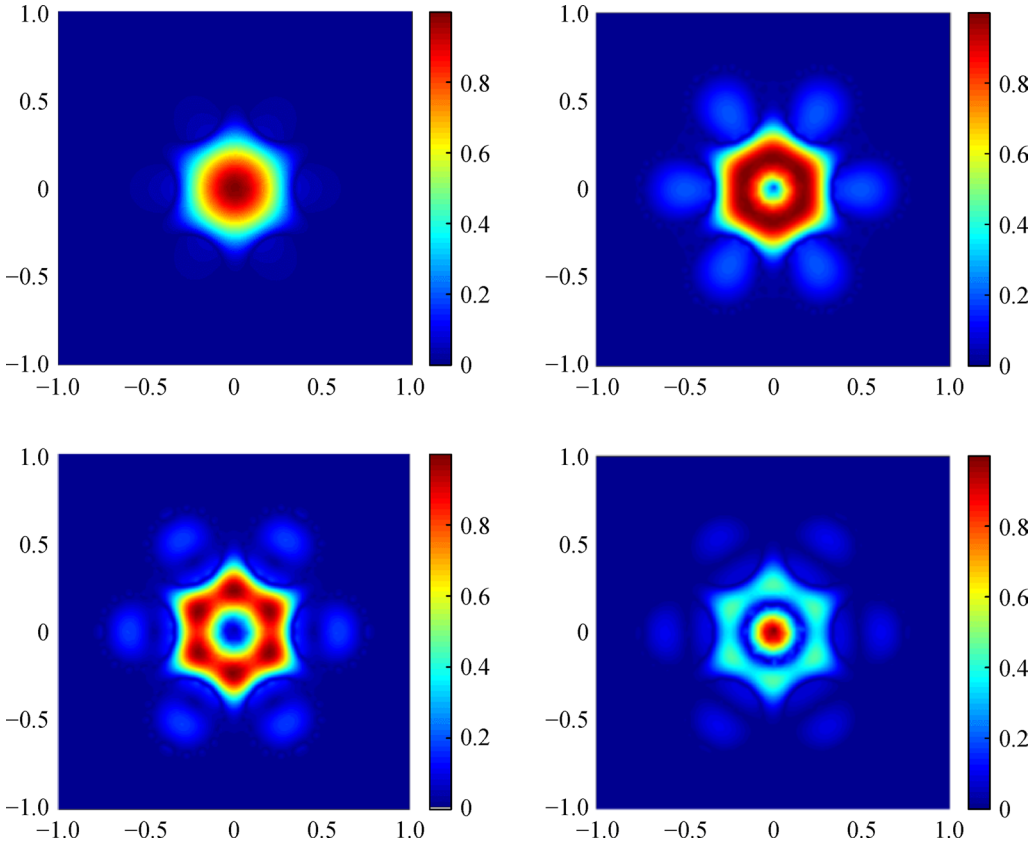

Fig. 3 Normalized intensity profiles of the AR-SCF. $n_1=1.89$, $n_2=2.20$, $D=30$ μm, $d=20$ μm, $N=6$, and $t=0.9$ μm, at wavelength of 2.8 μm

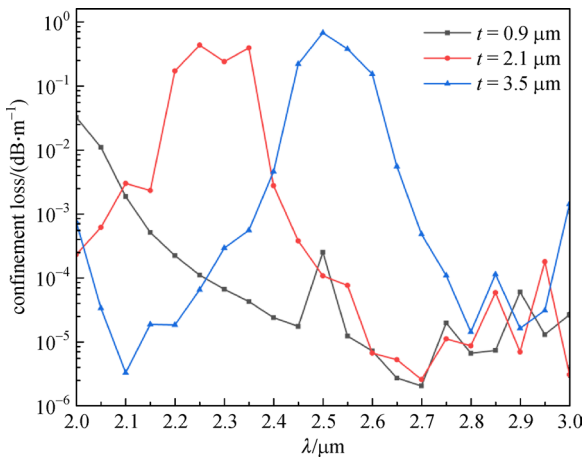

Fig. 4 Confinement loss (*CL*) with wavelength for different cladding-tube thickness (*t*). $n_1=1.89$, $n_2=2.20$, $D=30$ μm, $d=20$ μm

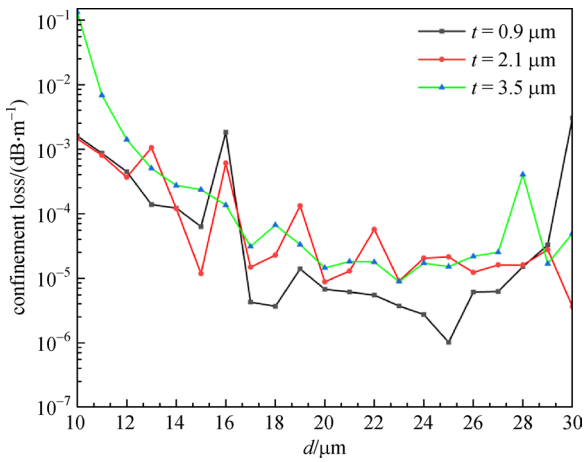

Fig. 5 Confinement loss (*CL*) with cladding-tube diameter for different cladding-tube thickness (*t*) at wavelength of 2.8 μm. $n_1=1.89$, $n_2=2.20$, $D=30$ μm, $d=20$ μm

d increase, and finally, the decrease appears fairly smooth. The *CL* of $t=3.5$ μm is larger than that of $t=0.9$ μm and $t=2.1$ μm. In the case of $t=0.9$ μm, the *CL* changes most gently with the *d*. The lowest *CL* appears at $t=0.9$ μm and $d=25$ μm. Therefore, the optimal structure of all-solid AR-SCF can be determined to be as follows: $n_1=1.89$, $n_2=2.20$, $D=30$ μm, $d=25$ μm, $N=6$, and $t=0.9$ μm, with the *CL* of 1.00623×10^{-6} dB/m, and number of guided mode of 4.

It is found that the value of *d* has no remarkable effect on the *CL* compared to the value of *t*. With that in mind, the design of the *d* can focus on the feasibility of fabrication.

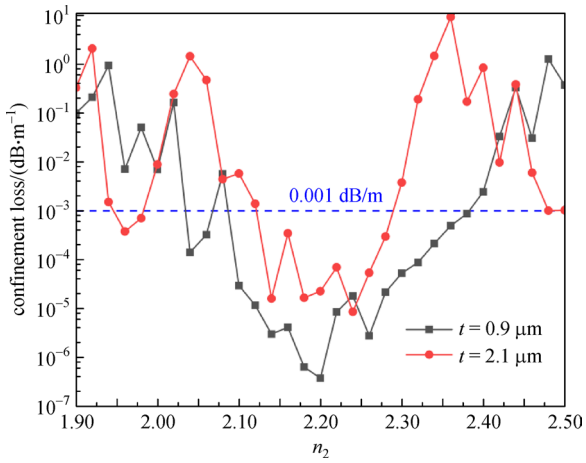

Fig. 6 Confinement loss (*CL*) with cladding-tube refractive index (n_2) for different cladding-tube thickness (t) at wavelength of 2.8 μm. $n_1 = 1.89$, $D = 30$ μm, $d = 25$ μm

To investigate the influence of different cladding tube materials, Fig. 6 presents the relationship between the *CL* and the cladding-tubes refractive index (n_2), with different cladding-tube thicknesses. With t as 0.9 and 2.1 μm, the n_2 varies from 1.90 to 2.50. We also see that the *CL* first decreases, then increases, with the increase of the n_2. The *CL* of $t = 0.9$ μm is lower than that of $t = 2.1$ μm. Considering 0.001 dB/m as the threshold for acceptable *CL* of AR-SCF, we can obtain the range of the n_2 under different t. When $t = 0.9$ and 2.1 μm, the ranges of n_2 are 2.06–2.38 and 2.16–2.28, respectively. Furthermore, there is little change in the number of guide modes as the value of n_2 varies. With the guide-mode number mainly stable at 4, we can see that n_2 takes on a smaller acceptable range as t increases.

Figure 7 depicts the relationship between the *CL* and the core refractive index (n_1) for different cladding-tube thicknesses. The t is 0.9 and 2.1 μm, the n_2 is 2.2, and the variation range of n_1 is from 1.60 to 1.90. We can see that when $n_1 \leq 1.85$, the *CL* decreases as the refractive index of the core increases, then increases gradually when $n_1 \geq 1.85$. Meanwhile, the overall *CL* of $t = 0.9$ μm is lower than the *CL* of $t = 2.1$ μm, and the number of guide modes is maintained at 4 constantly. If we consider 0.001 dB/m as the threshold, we can determine the value range of n_1 under different t. When $t = 0.9$ μm, the n_1 is varies from 1.66 to 1.90; when $t = 2.1$ μm, the n_1 is range from 1.78 to 1.90.

Next, we analyzed the influence of different fabrication errors on the value of *CL* and number of guided modes of AR-SCF. Figure 8 denotes the relationship between the *CL* and the cladding-tube thickness error (Δt). The cladding-tubes that have thickness error are represented in red in Fig. 9a, with N_e referring to the number of these cladding-tubes.

As Δt varies from 0 to 2.0 μm, the value of *CL* also changes periodically with little difference in N_e, as seen from the curve. However, the Δt greatly influences the AR-SCF mode. Figures 9b and 9c show the normalized intensity profiles of the fundamental and the second order mode when $\Delta t = 0.5$ μm and $N_e = 2$. From Fig. 9, we can see that the mode field of the fiber changes with the Δt, and the higher order modes changing more drastically. Therefore, the guide mode of the AR-SCF with cladding-tube thickness error is 2.

Using a similar approach, we analyzed the influence of different cladding-tube diameter errors (Δd) on the *CL* and number of guide modes. Figure 10 illustrates the relationship between the *CL* and the Δd with $N_e = 2$, 3 and 5. When the N_e is 2 and 3, Δd varied from −1.5 to 1.5 μm. When the N_e is 5, Δd varied within the range of −1.5–0.8 μm. The minus

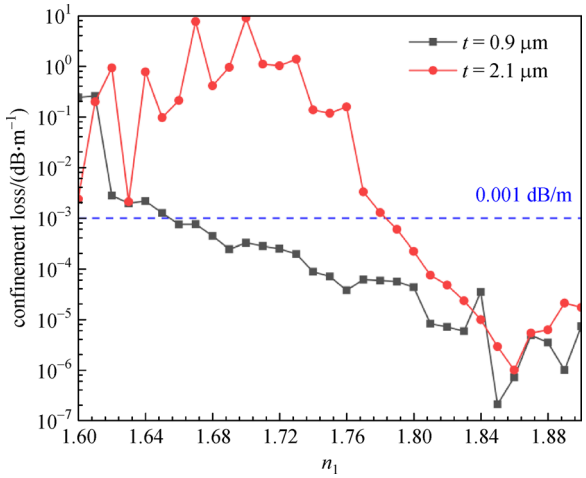

Fig. 7 Confinement loss (*CL*) with the core refractive index (n_1) for different cladding-tube thickness (t) at wavelength of 2.8 μm. $n_2 = 2.2$, $D = 30$ μm, $d = 25$ μm

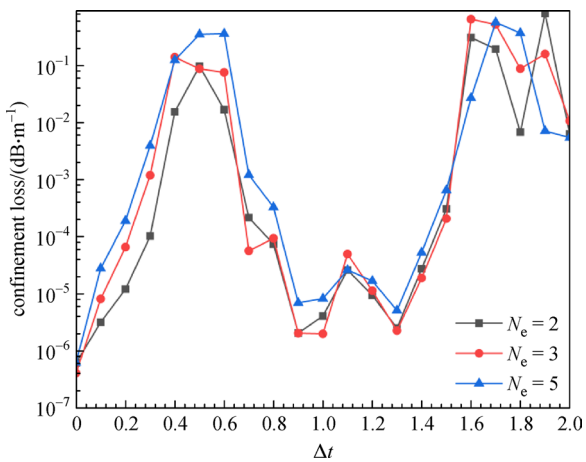

Fig. 8 Confinement loss (*CL*) with errors (Δt) of cladding-tube thickness for different cladding-tube number (N_e) at wavelength of 2.8 μm. $n_1 = 1.89$, $n_2 = 2.20$, $D = 30$ μm, $d = 25$ μm, $t = 0.9$ μm

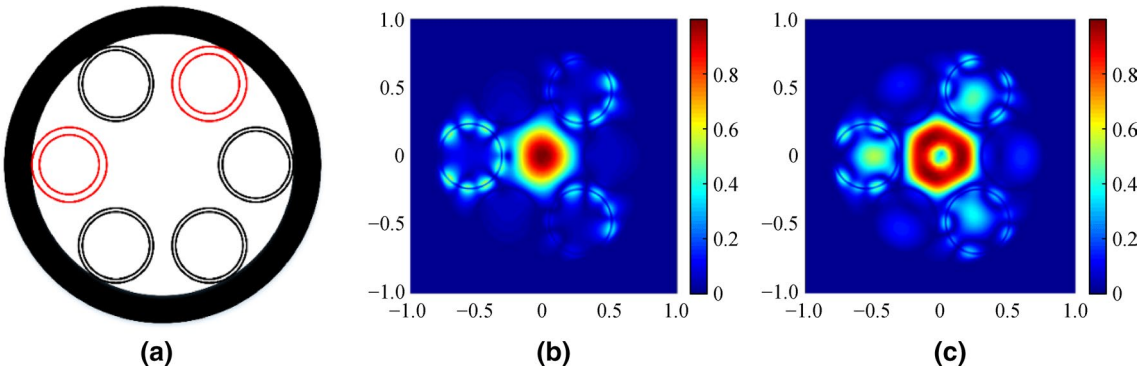

Fig. 9 AR-SCF structure with $\Delta t = 0.5$ μm, $N_e = 2$ **a**, and the normalized intensity profiles of fundamental mode **b** and second order mode **c**. $n_1 = 1.89$, $n_2 = 2.20$, $D = 30$ μm, $d = 25$ μm, and $t = 0.9$ μm, at wavelength of 2.8 μm

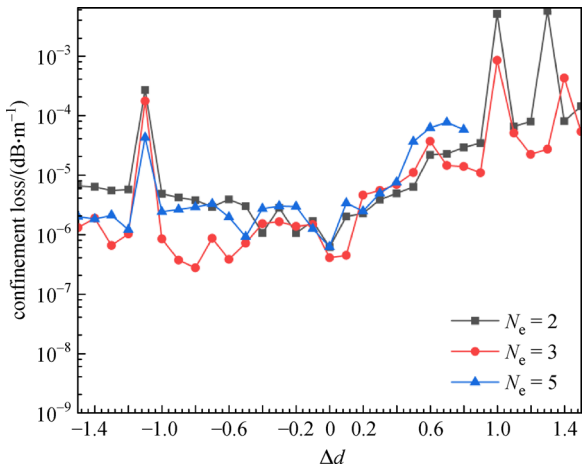

Fig. 10 Confinement loss (*CL*) with errors (Δd) of cladding-tube diameter for different cladding-tube number (N_e) at wavelength of 2.8 μm. $n_1 = 1.89$, $n_2 = 2.20$, $D = 30$ μm, $d = 25$ μm, $t = 0.9$ μm

sign indicates a smaller diameter and the plus sign indicates a larger diameter. As seen from Fig. 10, the variation trends of the three curves are essentially the same. The *CL* gradually increases as Δd increases, and the *CL* caused by the increase of diameter is greater than the decrease of diameter. Moreover, when the Δd exceeds ± 1.1 μm, the *CL* curve will show significant fluctuations. Therefore, we determined that the variation range of Δd is between -1.1 and 1.1 μm.

The effect of the Δd on the guide modes reported in Fig. 11 illustrates the normalized intensity profiles of the fundamental and second order mode, with $\Delta d = 0.5$ μm and $N_e = 3$. An increase in Δd changes the mode field, especially on the higher order mode, which decreases the number of guide modes from 4 to 2.

3.3 Discussion

The optimal structure parameters that attained by numerical simulation of the AR-SCF is $n_1 = 1.89$, $n_2 = 2.20$, $D = 30$ μm, $d = 25$ μm, $N = 6$, $t = 0.9$ μm, the *CL* and guide mode number is 1.00623×10^{-6} dB/m and 4, respectively. The fabrication of cladded single crystal fiber has been the main challenge faced during the application of single crystal fibers. However, we can expect to achieve the production of all-solid AR-SCF by improving the existing fabrication technology. The all-solid AR-SCF can be fabricated using the laser processing method. First, the single crystal core can be obtained using the edge-defined film-fed growth method (EFG) [34] and laser heated pedestal method (LHPG) [21]. Then, the cladding ring structure is etched using femtosecond laser processing technology [35]. Finally, the low melting point and high refractive index glass material is injected into the ring structure to prepare the fiber.

4 Conclusions

In this paper, we proposed a novel AR guiding SCF with high refractive index tubes cladding. By producing the cladding tubes using high refractive index material, AR guiding can be realized for SCFs, which can reduce the mode number to achieve single-mode and few-mode transmissions. First, we analyzed the feasibility of the anti-resonant light guiding mechanism, and results show that the all-solid single crystal fiber can realize that light guiding mechanism. We then discussed the influence of the AR-SCF structure parameter on confinement loss and guide modes, including the effect of wavelength, cladding-tube diameter, cladding material, and core material. Through our calculations, we determined the optimal structure to be: $n_1 = 1.89$, $n_2 = 2.20$, $D = 30$ μm, $d = 25.$μm, $N = 6$, and $t = 0.9$ μm with $CL = 1.00623 \times 10^{-6}$ dB/m and guide mode number is 4. Finally, we analyzed the influence of fabrication errors on confinement loss and number of guide modes, including the cladding-tube thickness error and cladding-tube diameter error. Additionally, we determined the tolerance range of

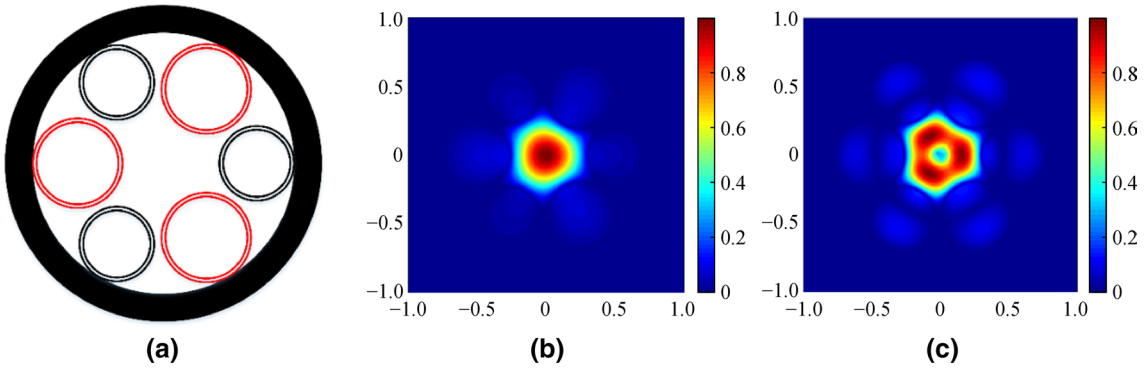

Fig. 11 AR-SCF structure with errors of cladding-tube diameter **a**, and the normalized intensity profiles of fundamental mode **b** and second order mode **c**. $n_1 = 1.89$, $n_2 = 2.20$, $D = 30$ μm, $d = 25$ μm, and $t = 0.9$ μm, at wavelength of 2.8 μm ($\Delta d = 0.5$ μm, $N_e = 3$)

fabrication error, providing a reference for the actual fabrication. In summary, our work would provide insight to new opportunities in the novel design of SCFs using different light-guiding techniques, which would greatly impact the field of laser application, supercontinum generation, and SCF sensors.

Acknowledgements This work was supported in part by the Fundamental Research Funds for the Central Universities (No. 2019JBM345), in part by the Beijing Natural Science Foundation (No. 4192047), and in part by the National Natural Science Foundation of China (Grant No. 61875064).

Authors' contributions JD is the designer and executor of this work. She has completed the data analysis and written the first draft of this manuscript; FM and XZ have participated in the simulation model design and data analysis of this work; XW, SQL, XS, and LY have test the simulation model, confirmed the correctness of the simulation results, analyzed numerical results, and revised the writing of the manuscript; GT and SL have contributed the ideas for this work, test of the numerical results, and written the manuscript. All authors have read and approved the final manuscript.

Declarations

Competing interests The authors declare that they have no competing interests.

References

1. Wang, T., Zhang, J., Zhang, N., Wang, S., Wu, B., Lin, N., Kusalik, P., Jia, Z., Tao, X.: Single crystal fibers: diversified functional crystal material. Adv. Fiber Mater. **1**(3–4), 163–187 (2019)
2. Luo, Q., Tang, G., Sun, M., Qian, G., Shi, Z., Qian, Q., Yang, Z.: Single crystal tellurium semiconductor core optical fibers. Opt. Mater. Express **10**(4), 1072 (2020)
3. Soleimani, N., Ponting, B., Gebremichael, E., Ribuot, A., Maxwell, G.: Coilable single crystals fibers of doped-YAG for high power laser applications. J. Cryst. Growth **393**, 18–22 (2014)
4. Kim W, Shaw B, Bayya S, Askins C, Peele J, Rhonehouse D, Meyers J, Thapa R, Gibson D, Sanghera J. Cladded single crystal fibers for high power fiber lasers. In: Proceedings of Photonic Fiber and Crystal Devices: Advances in Materials and Innovations in Device Applications X. San Diego: SPIE, 2016, 99580O
5. Yang, T.T., Yang, T.I., Soundararajan, R., Yeh, P.S., Kuo, C.Y., Huang, S.L., Donati, S.: Widely tunable, 25-mW power, Ti:sapphire crystal-fiber laser. IEEE Photonics Technol. Lett. **31**(24), 1921–1924 (2019)
6. Yin, S.S., Kim, J., Zhan, C., An, J., Lee, J., Ruffin, P., Edwards, E., Brantley, C., Luo, C.: Supercontinuum generation in single crystal sapphire fibers. Opt. Commun. **281**(5), 1113–1117 (2008)
7. Bezgabadi, A.S., Bolorizadeh, M.A.: Dispersion properties of a single-mode windmill single crystal sapphire optical fiber and its broadband infrared supercontinuum generation. Opt. Eng. **57**(11), 1 (2018)
8. Pfeiffenberger, N.: Sapphire photonic crystal fibers. Opt. Eng. **49**(9), 090501 (2010)
9. Hill, C., Homa, D., Liu, B., Yu, Z., Wang, A., Pickrell, G.: Submicron diameter single crystal sapphire optical fiber. Mater. Lett. **138**, 71–73 (2015)
10. Chen, H., Tian, F., Chi, J., Kanka, J., Du, H.: Advantage of multimode sapphire optical fiber for evanescent-field SERS sensing. Opt. Lett. **39**(20), 5822–5825 (2014)
11. Chen, H., Buric, M., Ohodnicki, P.R., Nakano, J., Liu, B., Chorpening, B.T.: Review and perspective: sapphire optical fiber cladding development for harsh environment sensing. Appl. Phys. Rev. **5**(1), 011102 (2018)
12. Myers J D, Kim W, Shaw L B, Bayya S, Qadri S N, Rhonehouse D, Askins C, Peele J, Thapa R, Bekele R Y, McClain C, Sanghera J S. Development of thin film claddings for single crystal optical fiber. In: Proceedings of Advanced Photonics 2018 (BGPP, IPR, NP, NOMA, Sensors, Networks, SPPCom, SOF). Zurich: OSA, NoTu4D.4 (2018)
13. Lai, C.C., Gao, W.T., Nguyen, D.H., Ma, Y.R., Cheng, N.C., Wang, S.C., Tjiu, J.W., Huang, C.M.: Toward single-mode active

crystal fibers for next-generation high-power fiber devices. ACS Appl. Mater. Interfaces. **6**(16), 13928–13936 (2014)
14. Bera S, Liu B, Wuenschell J K, Baltrus J, Lau D, Howard B, Buric M P, Chorpening B T, Ohodnicki P R. Fabrication and evaluation of sapphire fiber cladding via magnesium aluminate spinel sol-gel based approaches. In: Proceedings of Fiber Optic Sensors and Applications XVI. Baltimore: SPIE, 19 (2019)
15. Malinowski, M., Sarnecki, J., Piramidowicz, R., Szczepanski, P., Wolinski, W.: Epitaxial RE^{3+}:YAG planar waveguide lasers. Opto-Electron. Rev. **9**(1), 67–74 (2001)
16. Lo, C.Y., Huang, K.Y., Chen, J.C., Tu, S.Y., Huang, S.L.: Glass-clad Cr^{4+}:YAG crystal fiber for the generation of superwideband amplified spontaneous emission. Opt. Lett. **29**(5), 439–441 (2004)
17. Lo, C.Y., Huang, K.Y., Chen, J.C., Chuang, C.Y., Lai, C.C., Huang, S.L., Lin, Y.S., Yeh, P.S.: Double-clad Cr^{4+}:YAG crystal fiber amplifier. Opt. Lett. **30**(2), 129–131 (2005)
18. Huang, K.Y., Hsu, K.Y., Jheng, D.Y., Zhuo, W.J., Chen, P.Y., Yeh, P.S., Huang, S.L.: Low-loss propagation in Cr^{4+}:YAG double-clad crystal fiber fabricated by sapphire tube assisted CDLHPG technique. Opt. Express **16**(16), 12264–12271 (2008)
19. Tong, L., Gattass, R.R., Ashcom, J.B., He, S., Lou, J., Shen, M., Maxwell, I., Mazur, E.: Subwavelength-diameter silica wires for low-loss optical wave guiding. Nature **426**(6968), 816–819 (2003)
20. Lan, C.W., Tu, C.Y.: Three-dimensional simulation of facet formation and the coupled heat flow and segregation in bridgman growth of oxide crystals. J. Cryst. Growth **233**(3), 523–536 (2001)
21. Bera S, Nie C D, Harrington J A, Chick T, Chakrabarty A, Trembath-Reichert S, Chapman J, Rand S C. Cladding single crystal yag fibers grown by laser heated pedestal growth. In: Proceedings of Solid State Lasers XXV: Technology and Devices. San Francisco: SPIE, 97260C (2016)
22. Bufetova, G.A., Rusanov, S.Y., Seregin, V.F., Pyrkov, Y.N., Kamynin, V.A., Tsvetkov, V.B.: Temperature distribution across the growth zone of sapphire (Al_2O_3) and yttrium–aluminum garnet (YAG) single crystal fibers. J. Cryst. Growth **433**, 54–58 (2016)
23. Bufetova, G.A., Rusanov, S.Y., Seregin, V.F., Pyrkov, Y.N., Tsvetkov, V.B.: Temperature and emissivity measurements at the sapphire single crystal fiber growth process. J. Cryst. Growth **480**, 85–89 (2017)
24. Wang, W.L., Tseng, Y.H., Cheng, W.H., Wang, J.S.: Silica clad-ded Nd^{3+}:YAG single crystal core optical fiber and its submicron residual stress detection. Opt. Mater. Express **4**(4), 656 (2014)
25. Spratt, W., Huang, M., Murray, T., Xia, H.: Optical mode confinement and selection in single-crystal sapphire fibers by formation of nanometer scale cavities with hydrogen ion implantation. J. Appl. Phys. **114**(20), 203501 (2013)
26. Spratt, W.T., Huang, M., Jia, C., Wang, L., Kamineni, V.K., Diebold, A.C., Matyi, R., Xia, H.: Effects of hydrogen ion implantation and thermal annealing on structural and optical properties of single-crystal sapphire. Mater. Res. Soc. Online Proc. Lib. **1354**, 609 (2011)
27. Spratt, W.T., Huang, M., Jia, C., Wang, L., Kamineni, V.K., Diebold, A.C., Xia, H.: Formation of optical barriers with excellent thermal stability in single-crystal sapphire by hydrogen ion implantation and thermal annealing. Appl. Phys. Lett. **99**(11), 111909 (2011)
28. Wilson, B.A., Rana, S., Subbaraman, H., Kandadai, N., Blue, T.E.: Modeling of the creation of an internal cladding in sapphire optical fiber using the ^{6}Li(n, α)3H reaction. J. Lightwave Technol. **36**(23), 5381–5387 (2018)
29. Cheng, Y., Hill, C., Liu, B., Yu, Z., Xuan, H., Homa, D., Wang, A., Pickrell, G.: Design and analysis of large-core single-mode windmill single crystal sapphire optical fiber. Opt. Eng. **55**(6), 066101 (2016)
30. Hill, C., Homa, D., Yu, Z., Cheng, Y., Liu, B., Wang, A., Pickrell, G.: Single mode air-clad single crystal sapphire optical fiber. Appl. Sci. **7**(5), 473 (2017)
31. Wei, C., Joseph Weiblen, R., Menyuk, C.R., Hu, J.: Negative curvature fibers. Adv. Opt. Photon. **9**(3), 504 (2017)
32. Lian, X., Farrell, G., Wu, Q., Han, W., Shen, C., Ma, Y., Semenova, Y.: Anti-resonance, inhibited coupling and mode transition in depressed core fibers. Opt. Express **28**(11), 16526–16541 (2020)
33. Hossain, M. M., Maniruzzaman, M.: Analysis of dispersion and confinement loss in photonic crystal fiber. In: Proceedings of 2014 International Conference on Electrical Engineering and Information & Communication Technology. IEEE (2014)
34. Xu, S., Yao, Z., Pei, G., Luo, X., Wu, X., Lin, Y.: Preparation and properties of sapphire by edge-defined film-fed growth (EFG) method with different growth directions. J. Wuhan Univ. Technol. **33**(5), 1022–1027 (2018)
35. Maclean J O, Hodson J R, Voisey K T. Laser drilling of via microholes in single-crystal semiconductor substrates using a 1070 nm fibre laser with millisecond pulse widths. In: Proceedings of Industrial Laser Applications Symposium (ILAS 2015). Kenilworth: SPIE, 965704 (2015)

Jinmin Ding received her Bachelor's degree in Information Science and Engineering from University of Jinan, China, in 2019. She is currently pursuing the Ph.D. degree with Beijing Jiaotong University, China. Her research mainly focuses on special optical fibers.

Fanchao Meng received his Master's degree in Optical Engineering from Yanshan University, China, in 2019. He is currently pursuing the Ph.D. degree with Beijing Jiaotong University, China. His research mainly focuses on special optical fibers, and intelligent photonics.

Xiaoting Zhao received his Bachelor's degree in Computer Science and Technology from Anhui Agricultural University, China, in 2019. He is currently pursuing the Ph.D. degree with Beijing Jiaotong University, China. His research interests include research on big data analysis of fiber distributed sensor based on machine learning, and research on performance prediction and reverse design of microstructure fiber based on machine learning.

Xin Wang received her Ph.D. degree from Beijing Jiaotong University, China, in 2016. She is currently an Assosiate Professor in the School of Electronic and Information Engineering, Beijing Jiaotong University. Her current research interests include microstructured fiber, fiber laser and fiber sensor.

Shuqin Lou received her Ph.D. degree from Beijing Jiaotong University, China, in 2005. She is currently a fulltime Professor in the School of Electronic and Information Engineering, Beijing Jiaotong University. Her current research interests include microstructured fiber, fiber components, fiber laser, and fiber sensor.

Xinzhi Sheng received his Ph.D. degree in Physical Electronics and Optronics from Harbin Institute of Technology, China, in 1996. He is currently working as a professor at Beijing Jiaotong University, China. His research mainly focuss on optical fiber communication and sensing.

Luyun Yang is optical fiber manufacturing and research expert, associate professor of Wuhan National Laboratory for Optoelectronics, Huazhong University of Science and Technology, China. From 2006 to 2008, he was engaged in postdoctoral research in Japan; in 2012, he was an innovative entrepreneur in Kunshan, China; in 2019, he was an innovative "3551" entrepreneur in Wuhan, China; internationally, he was the first to prepare high concentration rare earth ion doped active optical fiber based on nano porous glass; he has published more than 100 papers in academic journals and conferences at home and abroad, presided over many projects such as National Natural Science Foundation of China, Key Scientific and Technological Research Projects of Hubei Province. His research interests include nanoporous materials, innovative MCVD technology, active fiber, micro-nano structure fiber, ultra wide band fiber amplification, fiber laser; especially good at the development of various types and structures of optical fiber.

Guangming Tao received his Ph.D. degree in Optics from the University of Central Florida, USA, in 2014. He was a Research Scientist/Senior research Scientist with The College of Optics and Photonics (CREOL), University of Central Florida, from 2014 to 2017. He was a Visiting Scholar with the Chinese Academy of Science from 2007 to 2008, the Massachusetts Institute of Technology in 2012, and the Centre National de la Recherche Scientifique in 2017. He is currently a Professor with the Wuhan National Laboratory for Optoelectronics, Huazhong University of Science and Technology (HUST), China, since 2017. He is the Director of the Center of Advanced Functional Fibers and the Director of the Man-Machine Laboratory (HUST) and the Director of Smart Fabric Hub of the China Textile Academy. He has authored about 60 scientific papers and holds more than 20 patents. He has given excess of 60 invited lectures/colloquia or keynote talks and has co-organized more than 10 national and international conferences and symposiua, including Symposium SM2 (Advanced Multifunctional Fibers and Textiles), the 2017 Spring MRS Meeting, Symposium J (Multifunctional and Multimaterial Fibers), the 2017 International Conference on Advanced Fibers and Polymer Materials, etc. He has years of research experience in optical science and engineering in academia, industry, and government institutes with expertise in the areas of functional fibers, smart fabric, man-machine interactions, specialty optical fibers, and in-fiber nano-fabrication.

Sheng Liang received his Ph.D. degree in Precision Instrument and Machinery from Beihang University, China, in 2011, for work on the fiber-optic distributed sensors. He is currently an Associate Professor with the Department of Physics, School of Science, Beijing Jiaotong University, China. His research mainly focuses on special optical fibers, and intelligent photonics.